Inorganic Chemistry

Article

pubs.acs.org/IC

Control of L-type Ferrimagnetism by the Ce/Vacancy Ordering in the *A*-Site-Ordered Perovskite $Ce_{1/2}Cu_3Ti_4O_{12}$

Takashi Saito,*[,†] Ryuta Yamada,[†] Clemens Ritter,[‡] Mark S. Senn,[§,∥] J. Paul Attfield,[§] and Yuichi Shimakawa[†,⊥]

[†]Institute for Chemical Research, Kyoto University, Gokasho, Uji, Kyoto 611-0011, Japan

[‡]Institut Laue-Langevin, BP 156, F-38042, Grenoble Cedex 9, France

[§]Centre for Science at Extreme Conditions and School of Chemistry, University of Edinburgh, Mayfield Road, Edinburgh EH9 3JZ, United Kingdom

[⊥]Japan Science and Technology Agency, CREST, Gokasho, Uji, Kyoto 611-0011, Japan

ABSTRACT: *A*-site-ordered perovskite $Ce_{1/2}Cu_3Ti_4O_{12}$ has been found to crystallize in two different forms, one with random and the other with ordered Ce/vacancy distribution at the *A* site of the prototype $AA'_3B_4O_{12}$ structure. The random phase is isostructural with $CaCu_3Ti_4O_{12}$, and the ordered phase is a new ordered derivative of the $AA'_3B_4O_{12}$-type perovskite with two crystallographically distinct Cu sites. Although both phases form a G-type antiferromagnetic arrangement of Cu^{2+} spins below 24 K, their magnetisms are quite different. A typical antiferromagnetic transition is observed in the random phase, whereas a small ferromagnetic moment appears below 24 K in the ordered phase, which rapidly decreases upon further cooling. A mean-field approximation approach revealed that this unusual behavior in the ordered phase is an L-type ferrimagnetism driven by the nonequivalent magnetizations of the two ferromagnetic Cu^{2+} spin sublattices in the G-type spin structure. This unusual ferrimagnetism is a direct consequence of the Ce/vacancy ordering.

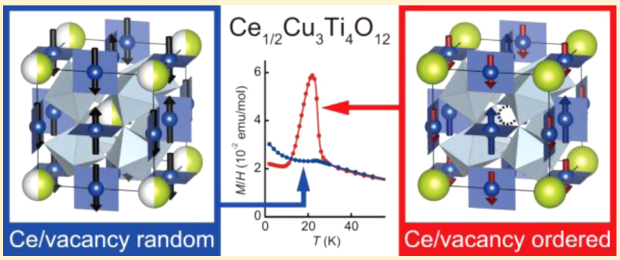

INTRODUCTION

A-site-ordered perovskites with the chemical formula $AA'_3B_4O_{12}$ show a wide variety of physical properties.[1−10] Their structure has an $a^+a^+a^+$-type octahedral rotation yielding square-planar-coordinated *A*′ sites at 3/4 of the originally 12-fold-coordinated *A* sites of the simple ABO_3 perovskite. Because the square-planar *A*′ sites can accommodate transition metal ions, such as Cu^{2+} and Mn^{3+}, electronic or magnetic correlations between *A*′ sites and between *A*′ sites and *B* sites are expected to play important roles in determining the physical properties of these compounds.

$CaCu_3Ti_4O_{12}$ is an antiferromagnetic (AFM) insulator that shows a giant dielectric constant over a wide temperature range.[2] It adopts the $Im\bar{3}$ space group symmetry, and the local Cu^{2+} spins with $S = 1/2$ at the square-planar *A*′ site undergo an AFM transition at a Néel temperature $T_N = 25$ K to form a G-type AFM spin structure in which all the nearest neighboring Cu^{2+} spins align antiparallel to each other.[11] The compound is a good target in which to investigate the *A*′−*A*′ magnetic interaction. Here the CuO_4 square units are isolated from each other, and the Ti-3d level is involved in the magnetic interactions, suggesting a Cu−O−Ti−O−Cu magnetic exchange path.[5,12] The crystal structures and the magnetism of $Ln_{2/3}Cu_3Ti_4O_{12}$ (*Ln* = lanthanide) compounds were reported recently.[13,14] These compounds all crystallize in the $Im\bar{3}$ space group with a random distribution of Ln^{3+} and vacancies at the *A* sites and with a $[Cu_3Ti_4O_{12}]^{2-}$ framework isostructural to that of $CaCu_3Ti_4O_{12}$. The magnetic behaviors of the *A*′-site Cu^{2+} spins in these compounds all closely resemble that of the *A*′-site Cu^{2+} spins in $CaCu_3Ti_4O_{12}$, exhibiting AFM transitions near 25 K, with only a very weak coupling of the paramagnetic and nonmagnetic lanthanide cations.

Among the $Ln_{2/3}Cu_3Ti_4O_{12}$ series, $Ce_{2/3}Cu_3Ti_4O_{12}$ could not be synthesized and $Ce_{1/2}Cu_3Ti_4O_{12}$ was obtained instead, probably because of the stability of Ce^{4+} at the *A* site.[13,15] Interestingly, the compound shows an anomalous magnetic transition in the magnetic susceptibility at about 24 K, which is very close to the T_N of AFM $CaCu_3Ti_4O_{12}$. However, neither the detailed low-temperature magnetic behavior nor the origin of the anomalous transition has been elucidated. In this study, therefore, detailed investigations on the crystal structure and the magnetic properties of $Ce_{1/2}Cu_3Ti_4O_{12}$ have been carried out. $Ce_{1/2}Cu_3Ti_4O_{12}$ was found to crystallize in two different forms, one with a random Ce/vacancy distribution and the other with Ce/vacancy ordering at the *A* sites. The magnetism was found to depend on the kind of distribution. The unusual temperature-dependent weak ferrimagnetism induced by the Ce/vacancy ordering is also discussed.

Received: October 16, 2013
Published: January 21, 2014

   dx.doi.org/10.1021/ic402616r | *Inorg. Chem.* 2014, 53, 1578−1584

EXPERIMENTAL SECTION

Two polycrystalline $Ce_{1/2}Cu_3Ti_4O_{12}$ samples, here denoted R- (random) and O- (ordered) CeCuTiO, were prepared by standard solid-state reaction as follows. A stoichiometric mixture of CeO_2, CuO, and TiO_2 (rutile) was calcined in flowing oxygen at 1000 °C and the mixture thus obtained was reground and pressed into pellets. R-CeCuTiO was prepared by heating a pellet to 1100 °C in air and cooling it rapidly by immersing it in liquid nitrogen, whereas O-CeCuTiO was prepared by heating a pellet to 1000 °C in flowing oxygen and cooling it to room temperature in 48 h.

Synchrotron X-ray diffraction (SXRD) experiments with the R- and O-CeCuTiO samples were performed at beamline BL02B2 of SPring-8 in Japan. Diffraction patterns at 300 K and a wavelength of 0.776 Å were recorded on imaging plates by using a Debye–Scherrer camera. Neutron diffraction (ND) experiments with both kinds of samples were performed at beamline D2B at the Institut Laue–Langevin in France. A constant wavelength of 1.549 Å was used, and diffraction patterns were collected at 2, 40, and 300 K for R-CeCuTiO and at 2, 20, 40, and 300 K for O-CeCuTiO. Rietveld refinements of the SXRD and ND patterns were performed with TOPAS and FULLPROF[16] programs, respectively.

Magnetic properties were measured using a SQUID magnetometer (MPMS, Quantum Design). Magnetic susceptibility in an external field of 1 T and isothermal magnetizations were measured. Heat capacity of the samples was also measured using a relaxation method (PPMS, Quantum Design).

RESULTS AND DISCUSSION

As shown in Figure 1a, the SXRD pattern of R-CeCuTiO at 300 K can be indexed with a 2 × 2 × 2 cubic supercell of a simple perovskite structure. The pattern was well reproduced in the Rietveld refinement with an $Im\bar{3}$ model isostructural with $CaCu_3Ti_4O_{12}$, indicating a random Ce/vacancy distribution at the unique *A* site. The refinement converged rapidly to an R_{wp} of 5.72% and a goodness of fit (GOF) of 1.33. The crystal structure obtained for R-CeCuTiO is shown in Figure 2a, the refined structural parameters are listed in Table 1a, and selected bond lengths and bond angles are listed in Table 2. R-CeCuTiO, with half of the 2*a* sites occupied by Ce, is isostructural with $CaCu_3Ti_4O_{12}$. The cation occupancies were fixed to the nominal ones, because only the stoichiometric $Ce_{1/2}Cu_3Ti_4O_{12}$ composition produced a nearly single phase sample. The bond valence sum (BVS) values for Cu and Ti calculated from the bond distances listed in Table 2 are 1.98 and 4.07, respectively, also confirming that the charge state is $Ce^{4+}_{1/2}Cu^{2+}_3Ti^{4+}_4O_{12}$.

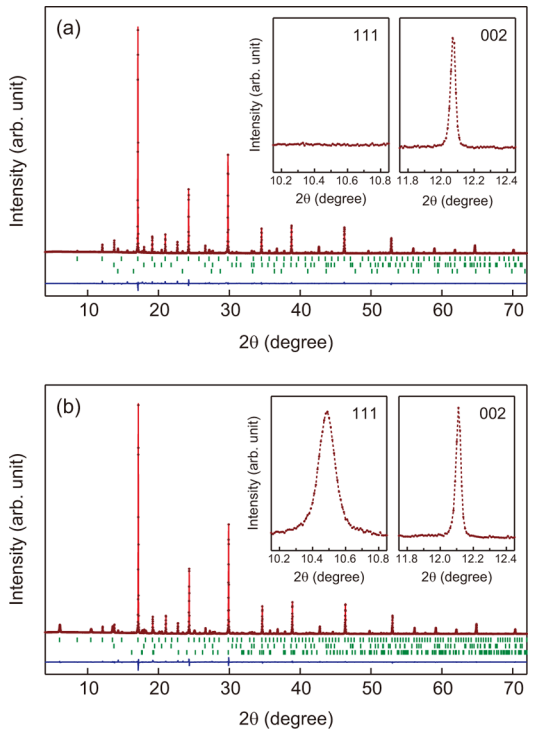

Figure 1. Rietveld plot of the SXRD patterns for (a) R-CeCuTiO and (b) O-CeCuTiO at room temperature. The observed (+), calculated (solid line), and difference (bottom) patterns are shown. The ticks indicate the allowed Bragg reflections. Small amounts of impurities (TiO_2 and CuO for R-CeCuTiO, and TiO_2 and CeO_2 for O-CeCuTiO) were included in the refinements. The insets show the expanded views for 111 (left) and 002 (right) reflections.

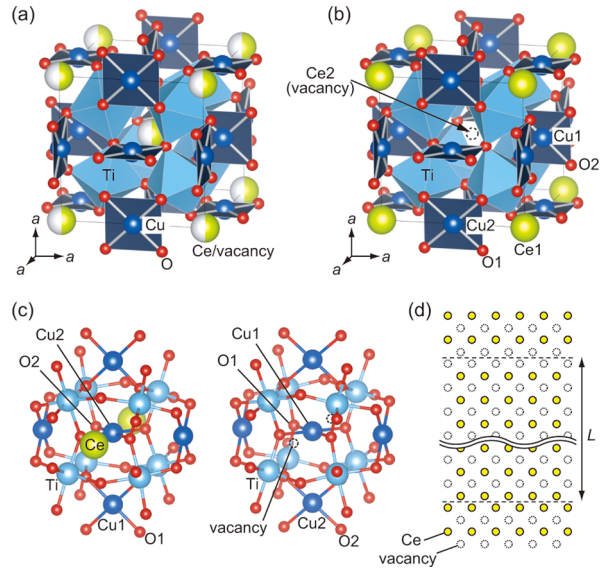

Figure 2. Crystal structures of (a) R-CeCuTiO and (b) O-CeCuTiO. The Ce site in R-CeCuTiO is half-occupied. (c) Local environments of Cu1 and Cu2 sites in O-CeCuTiO. (d) Schematic picture of O-CeCuTiO viewed from the [100] direction, where the Ce/vacancy sublattice forms antiphase boundaries. *L* represents the coherence length of the Ce/vacancy ordering.

The SXRD pattern of O-CeCuTiO at 300 K can also be indexed with the same cubic supercell as above, without any lowering of the crystal class, although *hkl* reflections with $h + k + l$ = odd violating the body-centered symmetry were clearly observed [Figure 1b]. This indicates the ordering of the Ce/vacancy distribution at the half-filled *A* sites of the prototype body-centered cubic $AA'_3B_4O_{12}$ structure. Among the maximal nonisomorphic subgroups of the $Im\bar{3}$ space group, only $Pm\bar{3}$ is compatible with such Ce/vacancy ordering, with cubic symmetry. The $Pm\bar{3}$ structure model was therefore used in the Rietveld refinement for O-CeCuTiO, and the refinement converged well with R_{wp} = 4.35% and GOF = 1.67. The refined structural parameters are listed in Table 1b, and selected bond lengths and bond angles are listed in Table 2. The $Pm\bar{3}$ structure model has two distinct crystallographic sites for each Ce, Cu, and O. Here the Ce occupancies were constrained as $g(Ce1) + g(Ce2) = 1$, to keep the stoichiometric $Ce_{1/2}Cu_3Ti_4O_{12}$ composition as in R-CeCuTiO. It should be noted that the obtained occupancies of the two Ce sites are significantly different: $g(Ce1)$ and $g(Ce2)$ is 0.935(2) and

dx.doi.org/10.1021/ic402616r | Inorg. Chem. 2014, 53, 1578–1584

Table 1. Results of the Rietveld Refinements of the SXRD Patterns for R- and O-CeCuTiO at Room Temperature[a]

(a) R-CeCuTiO						
atom	Wyck. pos.	x	y	z	g	B_{iso}
Ce	2*a*	0	0	0	1/2	0.38(1)
Cu	6*b*	0	1/2	1/2	1	0.38(1)
Ti	8*c*	1/4	1/4	1/4	1	0.76(1)
O	24*g*	0.3084(4)	0.1845(4)	0	1	0.28(3)
a = 7.39293(6) Å, R_{wp} = 5.35%, R_B = 2.54%, GOF = 1.24						
(b) O-CeCuTiO						
atom	Wyck. pos.	x	y	z	g	B_{iso}
Ce1	1*a*	0	0	0	0.935(2)	0.23(3)
Ce2	1*b*	1/2	1/2	1/2	0.065(2)	0.23(3)
Cu1	3*c*	0	1/2	1/2	1	0.39(1)
Cu2	3*d*	1/2	0	0	1	0.39(1)
Ti	8*i*	0.2561(1)	0.2561(1)	0.2561(1)	1	0.47(1)
O1	12*k*	0.3137(4)	1/2	0.1881(4)	1	0.17(7)
O2	12*j*	0.2980(4)	0.1757(4)	0	1	0.17(7)
a = 7.37852(3) Å, b = 0.080(1), R_{wp} = 4.35%, R_B = 1.68%, GOF = 1.67						

[a]Wyckoff position (Wyck. pos.), partial coordinates x, y, and z, site occupancy g, isotropic atomic displacement parameter B_{iso}, and lattice parameter a are listed, together with the reliability factors. The peak broadening parameter b is also given for O-CeCuTiO.

Table 2. Selected Bond Lengths and Bond Angles at Room Temperature for R- and O-CeCuTiO, obtained from the SXRD patterns

R-CeCuTiO		O-CeCuTiO	
Ce−O (×12), Å	2.657(2)	Ce1−O1 (×12), Å	2.681(3)
		Ce2−O2 (×4), Å	2.553(3)
Cu−O (×4), Å	1.967(2)	Cu1−O1 (×4), Å	1.953(3)
Cu−O (×4), Å	2.729(3)	Cu1−O2 (×4), Å	2.819(3)
Cu−O (×4), Å	3.261(2)	Cu1−O1 (×4), Å	3.264(2)
		Cu2−O2(×4), Å	1.975(3)
		Cu2−O1 (×4), Å	2.699(3)
		Cu2−O2 (×4), Å	3.250(3)
Ti−O (×6), Å	1.9587(9)	Ti−O1 (×3), Å	1.916(3)
		Ti−O2 (×3), Å	2.004(1)
Ti−O−Ti, deg	141.3(2)	Ti−O1−Ti, deg	139.9(2)
		Ti−O2−Ti, deg	141.02(6)
O−Ti−O, deg	88.3(1)/ 91.7(1)/ 180	O1−Ti−O1, deg	95.5(1)
		O1−Ti−O2, deg	89.8(1)/ 89.2(1)/ 172.5(1)
		O2−Ti−O2, deg	85.0(1)
Cu−O−Ti, deg	109.3(1)	Cu1−O1−Ti, deg	110.0(2)
		Cu2−O2−Ti, deg	108.1(1)

0.065(2), respectively. This site preference of Ce clearly shows the ordering of the Ce/vacancy distribution over the originally uniform A-sites of the prototype $AA'_3B_4O_{12}$ structure. The vacancy is located at the body-center position, and the Ti and O positions are slightly shifted from those in the $Im\bar{3}$ model. Both Cu1 and Cu2 have four short and eight long bonds, forming square-planar coordination by oxygen. The BVS values for Cu1, Cu2, and Ti are 2.03, 1.95, and 4.08, respectively, suggesting that the charge state is $Ce^{4+}_{1/2}Cu^{2+}_3Ti^{4+}_4O_{12}$ as in R-CeCuTiO. The A-site ordered perovskite $Ce_{1/2}Cu_3Ti_4O_{12}$ with Ce/vacancy ordering [Figure 2b] is a new ordered derivative of the $AA'_3B_4O_{12}$-type perovskite; $AA^*A'_3A''_3B_8O_{24}$ with A = Ce, A^* = vacancy (ideally), A' = A'' = Cu. The structural nonequivalence of A' and A'' sites [Figure 2(c)] plays the key role in the magnetism, as discussed below.

The non-body-centered reflections ($h + k + l$ = odd) of O-CeCuTiO in the SXRD pattern were significantly broader than the others, as shown in the inset of Figure 1b. Therefore, the peak width of these reflections were corrected by including an additional peak width contribution $B = b/\cos\theta$ in the Rietveld refinement. The coherence length L of the Ce/vacancy ordering in O-CeCuTiO can be evaluated from the Scherrer equation for size broadening, $B = K\lambda/L \cos\theta$, where λ is the wavelength and K is the shape factor. K is known to be 0.94 for spherical crystals with cubic symmetry.[17] The refined b value gives L = 91(1) Å, which is much shorter than the coherence length of the $[Cu_2Ti_4O_{12}]^{2-}$ particles suggested by the sharp body-centered reflections ($h + k + l$ = even). Therefore, the Ce/vacancy ordering at the body-centered cubic sublattice of the $AA'_3B_4O_{12}$ structure should form anti-phase boundaries within the $[Cu_2Ti_4O_{12}]^{2-}$ framework, as illustrated in Figure 2d. The results imply that the Ce/vacancy distribution in $Ce_{1/2}Cu_3Ti_4O_{12}$ is random at 1100 °C and disproportionates to form the Ce/vacancy ordering with the $Pm\bar{3}$ structure if the sample is cooled slowly. If the sample is quenched in liquid nitrogen, on the other hand, the random Ce/vacancy distribution persists at room temperature.

The R-CeCuTiO and O-CeCuTiO ND patterns obtained at 40 and 300 K were well reproduced in the Rietveld refinements with the $Im\bar{3}$ and $Pm\bar{3}$ models and are consistent with the above SXRD results. At 2 K, however, some non-body-centered reflections indicating a long-range magnetic ordering for R-CeCuTiO were observed [Figure 3a]. The R-CeCuTiO ND pattern obtained at 2 K was reproduced with an $Im\bar{3}$ crystal structure and an A'-site G-type AFM spin structure where all the nearest neighboring Cu^{2+} spins are aligned antiparallel. The magnetic propagation vector of the body-centered cubic cell is κ = [1 0 0], which is equivalent to κ = [0 1 0] or [0 0 1]. The magnetic moments were set along the a-axis, as it is not possible to determine the moment direction in a cubic system from powder ND patterns. The sizes of all the moments were constrained equivalent in the refinement, which was done to be consistent with the AFM behavior of the sample described below. The final results of the refinements are listed in Table 3. The refined magnetic moment M was 0.86(4) μ_B at 2 K, which is consistent with the S = 1/2 spin of divalent Cu. The obtained

dx.doi.org/10.1021/ic402616r | Inorg. Chem. 2014, 53, 1578−1584

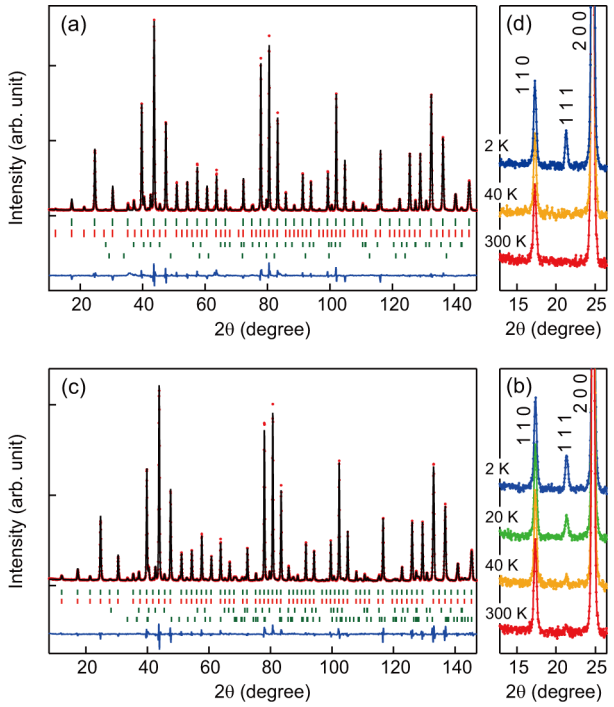

Figure 3. Rietveld plot of the ND patterns obtained at 2 K for (a) R-CeCuTiO and (c) O-CeCuTiO. The observed (+), calculated (solid line), and difference (bottom) patterns are shown, together with the ticks indicating the allowed nuclear (top low) and magnetic (second low) Bragg reflections. Small amounts of impurities (TiO_2 and CuO for R-CeCuTiO, and TiO_2 and CeO_2 for O-CeCuTiO) were included in the refinements. (b) and (d) show corresponding expanded views obtained between 300 and 2 K for R- and O-CeCuTiO, respectively.

spin structure (Figure 4) is identical to that reported for AFM $CaCu_3Ti_4O_{12}$. For O-CeCuTiO, the intensities of the same

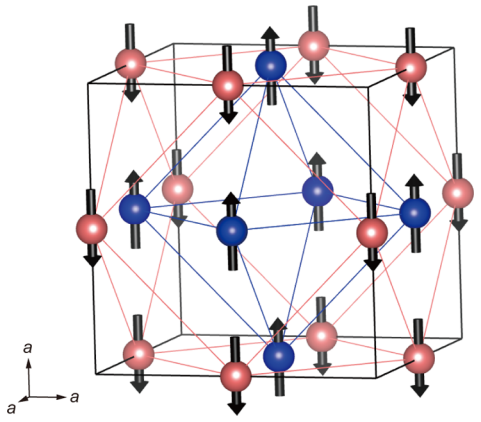

Figure 4. G-type AFM structure of R- and O-CeCuTiO at 2 K. Blue and pink spheres represent Cu sites with up and down spins, respectively, and each makes the FM spin sublattice.

reflections as in R-CeCuTiO increased below 20 K, as shown in Figure 3b, indicating the formation of a similar long-range magnetic ordering. The ND patterns obtained at both 20 and 2 K were well reproduced with a $Pm\bar{3}$ crystal structure and the same AFM spin structure described above, where ferromagnetic (FM) moments at Cu1 and Cu2 sublattices are coupled antiferromagnetically. The sizes of the Cu1/Cu2 sublattice moments were set to be identical in the refinement, because the spontaneous magnetization of the sample was very small, as also described below. The final results for the crystal and magnetic structures are listed in Table 3. The refined magnetic moment M was 0.85(3) μ_B at 2 K, which is also consistent with

Table 3. Results of the Rietveld Refinements of the ND Patterns for R- and O-CeCuTiO[a]

R-CeCuTiO				O-CeCuTiO				
	2 K	40 K	300 K		2 K	20 K	40 K	300 K
g(Ce)	1/2	1/2	1/2	g(Ce1)	0.935	0.935	0.935	0.935
B_{iso}(Ce), Å^2	0.20(2)	0.20(2)	0.47(2)	B_{iso}(Ce1), Å^2	0.15(9)	0.12(9)	0.10(1)	0.5(1)
				g(Ce2)	0.065	0.065	0.065	0.065
				B_{iso}(Ce2), Å^2	0.15(9)	0.12(9)	0.10(1)	0.5(1)
B_{iso}(Cu), Å^2	0.20(2)	0.20(2)	0.47(2)	B_{iso}(Cu1), Å^2	0.31(2)	0.31(2)	0.29(2)	0.53(2)
				B_{iso}(Cu2), Å^2	0.31(2)	0.31(2)	0.29(2)	0.53(2)
x(Ti)	1/4	1/4	1/4	x(Ti)	0.2546(1)	0.2547(4)	0.2550(4)	0.2550(4)
B_{iso}(Ti), Å^2	0.55(3)	0.52(3)	0.74(3)	B_{iso}(Ti), Å^2	0.41(3)	0.37(3)	0.32(3)	0.55(3)
x(O)	0.30419(9)	0.3042 (1)	0.3042(1)	x(O1)	0.3179(4)	0.3177(4)	0.3181(4)	0.3178(4)
y(O)	0.1803(1)	0.1801(1)	0.1803(1)	z(O1)	0.1915(2)	0.1914(2)	0.1916(2)	0.1914(3)
B_{iso}(O), Å^2	0.42(1)	0.40(1)	0.59(1)	B_{iso}(O1), Å^2	0.41(1)	0.40(1)	0.40(4)	0.56(1)
				x(O2)	0.2990(2)	0.2991(2)	0.2991(2)	0.2993(3)
				y(O2)	0.1779(4)	0.1777(4)	0.1782(4)	0.1783(4)
				B_{iso}(O2), Å^2	0.41(1)	0.40(1)	0.40(4)	0.56(1)
M, μ_B	0.86(4)			M, μ_B	0.85(3)	0.61(4)		
a, Å	7.38413(3)	7.38430(4)	7.39302[b]	a, Å	7.37014(3)	7.37015(3)	7.37027(4)	7.37879(4)
R_{wp}, %	6.69	6.91	6.55	R_{wp}, %	6.79	6.84	6.89	6.52
R_p, %	4.77	5.01	4.71	R_p, %	5.21	5.25	5.36	5.02
GOF	12.7	6.84	6.47	GOF	9.66	10.9	5.81	4.27

[a]The Wyckoff positions and partial coordinates of each atom are Ce 2a(0, 0, 0), Cu 6b(0, 1/2, 1/2), Ti 8c(1/4, 1/4, 1/4), and O 24g(x, y, 0) for R-CeCuTiO and are Ce1 1a(0, 0, 0), Ce2 1b(1/2, 1/2, 1/2), Cu1 3c(0, 1/2, 1/2), Cu2 3d(1/2, 0, 0), Ti 8i(x, x, x), O1 12k(x, 1/2, z), and O2 12j(x, y, 0) for O-CeCuTiO. Site occupancy g, isotropic atomic displacement parameter B_{iso}, partial coordinates x, y, and z, size of the magnetic moment M at Cu1/Cu2 sites, and lattice parameter a are listed together with the reliability factors. [b]The wavelength used for the measurements was calibrated using the lattice parameter of R-CeCuTiO obtained from the SXRD pattern at 300 K.

dx.doi.org/10.1021/ic402616r | Inorg. Chem. 2014, 53, 1578−1584

the $S = 1/2$ spin of divalent Cu, and it decreased to 0.61(4) μ_B at 20 K. Peak broadening of the non-body-centered reflections was not so obvious in ND because of the resolution limit of the diffractometer. Thus, the essential magnetic structure of O-CeCuTiO is the same as that of R-CeCuTiO (G-type AFM).

Figure 5 shows the temperature dependence of the magnetic susceptibility χ of R- and O-CeCuTiO measured under a magnetic field of 1 T. The observed χ obeys the Curie–Weiss law at high temperatures, and the fitting of these data above 100 K gives a Curie constant $C = 1.319(6)$ emu/(mol K) and a Weiss temperature $\theta_{CW} = -28.3(4)$ K for R-CeCuTiO, and $C = 1.259(3)$ emu/(mol K) and $\theta_{CW} = -26.4(2)$ K for O-CeCuTiO. There are no apparent contributions from Ce^{3+} and/or Ti^{3+} magnetic ions, which would be present if the samples have off-stoichiometry. These values are very similar to those for $CaCu_3Ti_4O_{12}$: $C = 1.365$ emu/(mol K) and $\theta_{CW} = -32.6$ K.[5] The results suggest the existence of local Cu^{2+} spins with $S = 1/2$ at the Cu sites for both R- and O-CeCuTiO, which is consistent with the above BVS calculations and the ND magnetic structure refinements. The results also indicate AFM interactions between the A'-site Cu spins in these compounds and that the magnitude of this interaction is similar to that in AFM $CaCu_3Ti_4O_{12}$. For R-CeCuTiO, an AFM transition is clearly observed at 24 K, which is also very close to the T_N for $CaCu_3Ti_4O_{12}$. The resemblance of the magnetism of R-CeCuTiO to that of $CaCu_3Ti_4O_{12}$ indicates that the random Ce/vacancy distribution at the 2*a* sites does not affect the magnetism of the Cu^{2+} spin sublattice. On the other hand, χ of O-CeCuTiO shows a sharp increase followed by a sharp decrease with decreasing temperature, as reported previously.[11] This behavior differs remarkably from the AFM transitions in R-CeCuTiO and $CaCu_3Ti_4O_{12}$ even though it occurs at a temperature very close to T_N of those compounds. It is clear from the temperature dependence of the heat capacity of O-CeCuTiO, shown in the inset of Figure 5, that there is only one phase transition related to the anomaly in the magnetic susceptibility and that it occurs at $T_M = 24$ K. The anomaly in χ should thus be related to the development of the AFM spin structure obtained by ND. It is to be noted that the magnetic behaviors of R- and O-CeCuTiO are very different near their transition temperatures even though the magnetic structures of their ground states are essentially the same.

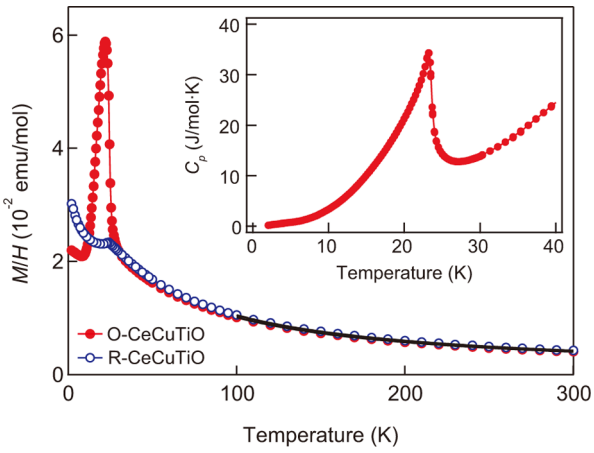

Figure 5. Temperature dependence of the magnetic susceptibility of (○) R-CeCuTiO and (●) O-CeCuTiO in a magnetic field of 1 T. For both cases the results of the Curie–Weiss fitting above 100 K are shown by thick black lines. Temperature dependence of the specific heat of O-CeCuTiO is shown in the inset.

The details of such an unusual transition behavior were further investigated by measuring the isothermal magnetization of O-CeCuTiO near T_M, as shown in Figure 6. The observed magnetization shows linear field dependence above 26 K and below 12 K but has a FM component between those temperatures. Spontaneous magnetization M_0, obtained by extrapolating the magnetization above 2 T to zero field, apparently develops only in the vicinity of T_M. As shown in Figure 7, M_0 increases sharply below T_M, decreases below 22 K, and vanishes around 10 K. This temperature dependence resembles that of χ measured at 1 T. Because O-CeCuTiO has two distinct crystallographic Cu sites each forming a magnetic sublattice, the two sublattices cannot be perfectly canceled out antiferromagnetically. We thus consider a two-sublattice ferrimagnetic model in which two FM sublattices of Cu1 and Cu2 are coupled antiferromagnetically and the sublattice moments have slightly different temperature dependences. In such a case, the size of the FM sublattice moments of the Cu1 and Cu2 will be different near the magnetic ordering temperature, producing a small noncompensated ferromagnetic moment. The ferromagnetic moment is expected to vanish on further cooling, as the Cu1/Cu2 sublattice moments saturate to an identical value. Such a magnetism is called L-type ferrimagnetism, as reported for $Fe_2(SO_4)_3$, $Fe_2(MoO_4)_3$ and α-$Li_3Fe_2(PO_4)_3$.[18−23]

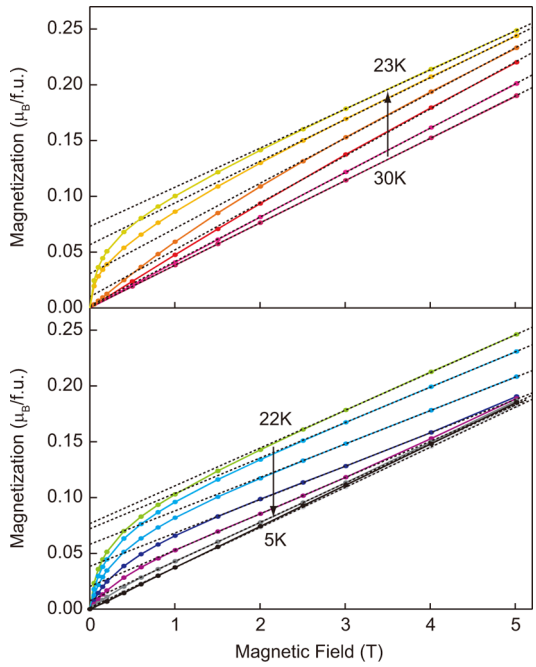

Figure 6. Isothermal magnetization of O-CeCuTiO. Data at 30, 28, 26, 25, 24, and 23 K are shown in the upper panel, and data at 22, 20, 18, 16, 14, 12, 10, and 5 K are shown in the lower panel. Extrapolation of the data above 2 T to zero-field is shown by dotted lines.

The temperature dependence of M_0 in O-CeCuTiO was fitted to the two-sublattice AFM model using a mean–field approximation.[24,25] Because M_0 is nearly zero below 10 K, the sublattice saturation moments M_s at both sites were set to be identical. The sublattice magnetization M_i ($i = 1, 2$) in a sublattice field H_i at a temperature T can be expressed using the Brillouin function B_S as

dx.doi.org/10.1021/ic402616r | Inorg. Chem. 2014, 53, 1578−1584

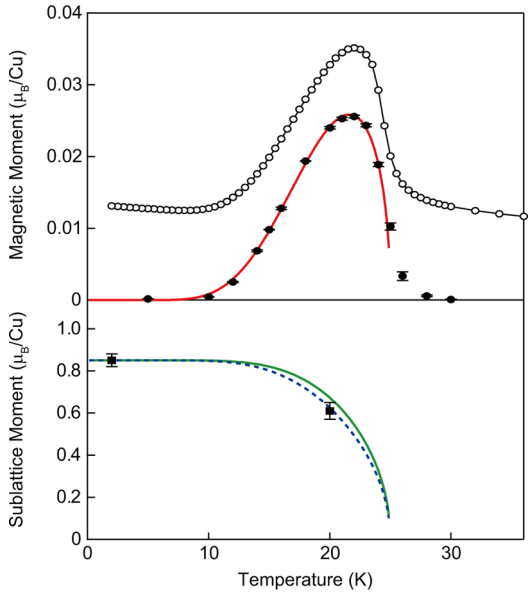

Figure 7. Temperature dependence of (●) the spontaneous magnetization M_0 and (○) the magnetization measured under 1 T for O-CeCuTiO are plotted in the upper panel. The sublattice moments refined from the ND patterns for O-CeCuTiO obtained at 2 and 20 K are plotted in the lower panel, where the sublattice magnetizations calculated from eq 5 are plotted with solid and dashed lines. The net magnetization per Cu, obtained from the difference between the two sublattice moments, is also shown in the upper panel with a solid line.

$$M_i = M_s B_S(gS\mu_B H_i/k_B T) \quad (1)$$

where g is the Landé g-factor, μ_B the Bohr magneton, and k_B the Boltzmann constant. For an $S = 1/2$ system it is expressed as

$$M_i = M_s \tanh(g\mu_B H_i/2k_B T) \quad (2)$$

If we assume that the H_i for both sites in a zero-field below a critical point T_C can be approximated with a single critical exponent β and an effective mean field constant λ_i at each site as

$$H_i = \lambda_i(1 - T/T_C)^\beta \quad (3)$$

we obtain

$$M_i = M_s \tanh\{(g\mu_B\lambda_i/2k_B T)(1 - T/T_C)^\beta\} \quad (4)$$

In this model with two antiparallel FM spin sublattices, the net magnetic moment M in a zero-field can be expressed as

$$\begin{aligned} M &= M_1 - M_2 \\ &= M_s[\tanh\{(A_1/T)(1 - T/T_C)^\beta\} \\ &\quad - \tanh\{(A_2/T)(1 - T/T_C)^\beta\}] \end{aligned} \quad (5)$$

where $A_i = g\mu_B\lambda_i M_S/2k_B$. The experimentally observed temperature dependence of M_0 from 5 to 25 K was fitted to this formula while fixing M_s to 0.85 μ_B as obtained in the ND analysis. The result is shown in Figure 7, and the refined values are $A_1 = 47(1)$ K, $A_2 = 41(1)$ K, $\beta = 0.49(3)$ and $T_C = 25.0(2)$ K. The obtained T_C well matches the T_M obtained above, and β is close to the theoretical value for the classical mean field model ($\beta = 0.5$).[26] As shown in Figure 7, the temperature dependences of M_1 and M_2 calculated from eq 5 are slightly different below T_C but converge to the same limit below ~10 K. The values at 20 K are both very close to the value obtained from the ND analysis which is also plotted in Figure 7.

The results confirm that the anomalous magnetism of O-CeCuTiO can be explained using the above two-sublattice AFM model. The difference in A_i for Cu1/Cu2 sublattices originates from the crystallographic difference in their environments (Table 2). The magnetic exchange paths for Cu1/Cu2 spins are influenced by the Ce/vacancy ordering [Figure 2c,d], and such differences in the local structure should induce a slight difference in the intrasublattice FM interactions. Although the ground state AFM structure of O-CeCuTiO is the same as that of R-CeCuTiO, with identical $S = 1/2$ spins at both Cu1 and Cu2 sites, the difference in the intrasublattice interactions causes the difference in the temperature evolution of the sublattice moments. Consequently, the anomalous behavior of the FM-like increase in the magnetization appears only in the vicinity of the transition temperature. We note here again that such weak ferrimagnetism is observed only in O-CeCuTiO, and normal AFM behavior is observed in R-CeCuTiO instead. It is therefore concluded that the Ce/vacancy ordering is the origin of the unusual magnetic behavior in O-CeCuTiO and that the ordering induces such L-type ferrimagnetism in $Ce_{1/2}Cu_3Ti_4O_{12}$.

■ CONCLUSIONS

A-site-ordered perovskites with a composition $Ce_{1/2}Cu_3Ti_4O_{12}$ were prepared in two forms. R-CeCuTiO has a random Ce/vacancy distribution with $Im\bar{3}$ symmetry, whereas O-CeCuTiO has a Ce/vacancy ordering with $Pm\bar{3}$ symmetry. R-CeCuTiO is isostructural with $CaCu_3Ti_4O_{12}$ and, like the AFM $CaCu_3Ti_4O_{12}$, undergoes a G-type AFM ordering of Cu^{2+} local spins below 24K. In O-CeCuTiO, on the other hand, Ce/vacancy ordering at the half-occupied *A* sites of the prototype $AA'_3B_4O_{12}$ structure produces two crystallographically distinct sites for Cu. The Cu1 and Cu2 sites with local spin $S = 1/2$ each form a FM sublattice and they are coupled antiferromagnetically, also forming a G-type AFM structure below 24 K. The Ce-ordering in O-CeCuTiO, however, induces a difference in the magnetic exchange fields at the FM Cu1/Cu2 sublattices, resulting in a nonequivalent evolution of the sublattice moments below the transition temperature. This accounts for the unusual appearance and rapid disappearance of the spontaneous magnetization. Magnetic interactions in $Ce_{1/2}Cu_3Ti_4O_{12}$ are sensitive to the Ce/vacancy distribution at the *A* sites, and whether the distribution is random or ordered determines whether the magnetism is simple antiferromagnetism or rather rare L-type ferrimagnetism.

■ AUTHOR INFORMATION

Corresponding Author

*T. Saito. E-mail: saito@scl.kyoto-u.ac.jp.

Present Address

[‖]Diamond Light Source Ltd., Didcot, Oxfordshire OX11 0DE, United Kingdom

Author Contributions

The paper was written through contributions of all authors.

Notes

The authors declare no competing financial interest.

■ ACKNOWLEDGMENTS

This work was done under the Strategic Japanese−UK Cooperative Program by JST/EPSRC. The SXRD experiments

were performed with the approval of the Japan Synchrotron Radiation Research Institute (Proposal No. 2012A-1588). The work was partly supported by the Global COE Program No. B09, Grants-in-Aid for Scientific Research (Grants Nos. 19GS0207 and 22740227), a grant for the Joint Project of Chemical Synthesis Core Research Institutions from MEXT, and a JST-CREST program of Japan. Support was also provided by EPSRC and STFC, United Kingdom.

REFERENCES

(1) Zeng, Z.; Greenblatt, M.; Subramanian, M. A.; Croft, M. *Phys. Rev. Lett.* **1999**, *82*, 3164.
(2) Subramanian, M. A.; Sleight, A. W. *Solid State Sci.* **2002**, *4*, 347.
(3) Prodi, A.; Gilioli, E.; Gauzzi, A.; Licci, F.; Marezio, M.; Bolzoni, F.; Huang, Q.; Santoro, A.; Lynn, J. W. *Nature Mat.* **2004**, *3*, 48.
(4) Kobayashi, W.; Terasaki, I.; Takeya, J.; Tsukada, I.; Ando, Y. *J. Phys. Soc. Jpn.* **2004**, *73*, 2373.
(5) Shiraki, H.; Saito, T.; Yamada, T.; Tsujimoto, M.; Azuma, M.; Kurata, H.; Isoda, S.; Takano, M.; Shimakawa, Y. *Phys. Rev. B* **2007**, *460*, 420.
(6) Vasil'ev, A. N.; Volkova, O. S. *Low Temp. Phys.* **2007**, *33*, 895.
(7) Shiraki, H.; Saito, T.; Azuma, M.; Shimakawa, Y. *J. Phys. Soc. Jpn.* **2008**, *77*, 64705.
(8) Yamada, I.; Takata, K.; Hayashi, N.; Shinohara, S.; Azuma, M.; Mori, S.; Muranaka, S.; Shimakawa, Y.; Takano, M. *Angew. Chem., Int. Ed.* **2008**, *47*, 7032.
(9) Shimakawa, Y. *Inorg. Chem.* **2008**, *47*, 8562.
(10) Long, Y. W.; Hayashi, N.; Saito, T.; Azuma, M.; Muranaka, S.; Shimakawa, Y. *Nature* **2009**, *458*, 60.
(11) Kim, Y. J.; Wakimoto, S.; Shapiro, S. M.; Gehring, P. M.; Ramirez, A. P. *Solid State Commun.* **2002**, *121*, 625.
(12) Mizumaki, M.; Saito, T.; Shiraki, H.; Shimakawa, Y. *Inorg. Chem.* **2009**, *48*, 3499.
(13) Dittl, A.; Krohns, S.; Sebald, J.; Schrettle, F.; Hemmida, M.; Krug von Nidda, H.-A.; Riegg, S.; Reller, A.; Ebbinghaus, S. G.; Loidl, A. *Eur. Phys. J. B* **2011**, *79*, 391.
(14) Shimakawa, Y.; Saito, T. *Physica Status Solidi B* **2012**, *249*, 423.
(15) Bochu, B.; Deschizeaux, M. N.; Joubert, J. C.; Collomb, A.; Chenavas, J.; Marezio, M. *J. Solid State Chem.* **1979**, *29*, 29.
(16) Wiles, D. B.; Young, R. A. *J. Appl. Crystallogr.* **1981**, *14*, 149.
(17) Langford, J. I.; Wilson, A. J. C. *J. Appl. Crystallogr.* **1978**, *11*, 102.
(18) Long, G. J.; Longworth, G.; Battle, P.; Cheetham, A. K.; Thundathil, R. V.; Beveridge, D. *Inorg. Chem.* **1979**, *18*, 624.
(19) Culvahouse, J. W. *J. Magn. Magn. Mater.* **1980**, *21*, 133.
(20) Jirak, Z.; Salmon, R.; Fournes, L.; Menil, F.; Hagenmuller, P. *Inorg. Chem.* **1982**, *21*, 4218.
(21) Battle, P. D.; Cheetham, A. K.; Long, G. J.; Longworth, G. *Inorg. Chem.* **1982**, *21*, 4223.
(22) Goñi, A.; Lezama, L.; Moreno, N. O.; Fournès, L.; Olazcuaga, R.; Barberis, G. E.; Rojo, T. *Chem. Mater.* **2000**, *12*, 62.
(23) Néel, L. *Ann. Phys.* **1948**, *3*, 137.
(24) Goodenough, J. B.; *Magnetism and the chemical bond*; John Wiley & Sons: New York, 1963.
(25) Goñi, A.; Lezama, L.; Moreno, N. O.; Fournès, L.; Olazcuaga, R.; Barberis, G. E.; Rojo, T. *Chem. Mater.* **2000**, *12*, 62.
(26) Landau, L. D. *Zh. Eksp. Teor. Fiz.* **1937**, *7*, 19.